Nano Energy 66 (2019) 104137

Contents lists available at ScienceDirect

Nano Energy

journal homepage: http://www.elsevier.com/locate/nanoen

Communication

Superior performance of half-wave to full-wave rectifier as a power conditioning circuit for triboelectric nanogenerators: Application to contact-separation and sliding mode TENG

Ali Ghaffarinejad [a,b], Javad Yavand Hasani [b,*], Dimitri Galayko [c], Philippe Basset [a,**]

[a] Université Paris-Est, ESYCOM, ESIEE Paris-CNAM-UPEM, Noisy-le-Grand, 93162, France
[b] School of Electrical Engineering, Iran University of Science and Technology, Tehran, 16846-13114, Iran
[c] Sorbonne Universités, F-75005, Paris, France

ARTICLE INFO

Keywords:
Triboelectric nanogenerator
Power conditioning circuit
Half-wave and full-wave rectifiers

ABSTRACT

In this brief communication the performance of a half-wave rectifier is compared with a full-wave rectifier as a conditioning circuit (CC) for a triboelectric nanogenerator (TENG) in providing electrical energy to a capacitive load. Contrary to the common understanding, it is shown that half-wave circuit provides a higher maximum energy to the capacitive load compared to full-wave. Formulas are provided to calculate the maximum energy delivered by the TENG to a capacitive load. Theoretical results show the enhanced performance of the half-wave CC compared to the full-wave. A TENG working in contact-separation mode is fabricated and tested with both CC's and experimental results show a very good agreement with theoretical derivations, and confirm that half-wave CC provides a higher energy to the load compared to full-wave. The outcomes of this report should be useful for the researchers working on the development of CC's for TENG's.

1. Introduction

Triboelectric nanogenerators (TENG's) are a promising technology to power-up low-power consumer electronics and medical devices [1,2]. Such transducers have been developed for years and the research for developing new TENG's is still going on [3,4]. However, the output power of such transducers are still low and a huge interest exists for the design and development of new and enhanced conditioning circuits to boost the output performance of TENG's [5,6]. Conditioning circuits are an essential part of a kinetic energy conversion system that can control and amplify the flow of energy from one domain to another [7–9]. Usually, a CC for TENG include a rectifying circuit or element such as diodes and switches to convert the alternating output current of the device into a direct current that can be stored in a reservoir capacitance [9–11]. There are vast ranges of applications for TENG's that are dependent to the implementation of conditioning circuits. Applications include self-powered electronic and photosynthetic bio-electronic sensors, green electronic skins, scavenging free energies from rain drops and water waves and body-heat energy converters, just to name a few among many examples [12–17].

Half-wave and full-wave rectifiers, among all, are the most widely used conditioning circuits in developing TENG. Therefore, several attempts have been made to enhance the performance of these two circuits. In [18], researchers tried adding serial and parallel switches in combination to a full-wave rectifier to enhance the output performance of a TENG. In [19], researchers mixed the full-wave rectifier with a transformer to boost the output power. In [20], a two stage logically-controlled switching system is used in combination with a full-wave rectifier and coupled inductors to manage the output power of the TENG. In [21], researchers employed a MOSFET switch controlled by a comparator as the next stage to a full-wave rectifier to manage the charge flow from the T-ENG. Nearly in all the cases, full-wave rectifier is chosen over the half-wave as a CC since it is believed by the researchers of the field that a full-wave CC delivers a higher energy to the load compared to the half-wave CC. In this short report, we will show that half-wave circuit delivers a higher energy per cycle of the operation of the TENG to a capacitive load compared to the full-wave rectifier. However, it should be noticed that the outcomes of this work are only applicable to the kinds of triboelectric nanogenerators that have variable capacitance values, such as contact-separation (CS) and

* Corresponding author.
** Corresponding author.
E-mail addresses: yavand@iust.ac.ir (J. Yavand Hasani), philippe.basset@esiee.fr (P. Basset).

https://doi.org/10.1016/j.nanoen.2019.104137
Received 27 June 2019; Received in revised form 31 August 2019; Accepted 24 September 2019
Available online 26 September 2019
2211-2855/

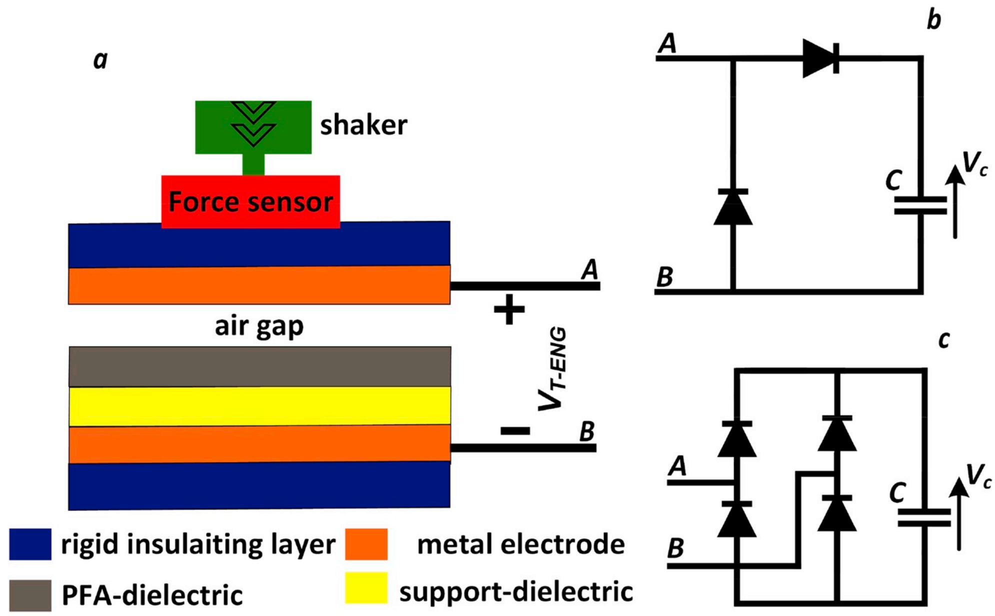

Fig. 1. a. the contact-separation mode TENG fabricated for the experiments with PFA as the dielectric layer. b. half-wave and c. full-wave rectifiers as CC for the TENG to charge the capacitor load of C.

lateral-sliding (LS) types.

2. Theoretical development

Fig. 1 shows a description of the contact-separation mode TENG and the two conditioning circuits under study. Two dielectric layers are attached onto the bottom electrode of the TENG that is fixed, and the top electrode is actuated by a magnetic shaker in the vertical direction with a sinusoidal excitation. As the top electrode touches the dielectric surface, negative triboelectric charges are generated on the surface and positive charges are induced on the top and bottom electrodes. The output ports of A and B of the TENG will be connected to the corresponding ports of the two conditioning circuits.

The total energy of the capacitor in the i^{th} cycle is defined as $W_i = 0.5CV_{C\_i}^2$ and the converted energy during the i^{th} cycle is defined as $\Delta W_i = W_{i+1} - W_i$ [22]. In case the TENG is connected to the half-wave rectifier as in Fig. 1b, the converted energy can be formulised as [22] (Section S2 of supporting information):

$$\Delta W_{i\_HW} = V_{TE}V_{C\_i}C_{max}\left(1 - \frac{1 + V_{C\_i}/V_{TE}}{C_{max}/C_{min}}\right) \tag{1}$$

where V_{TE} is the constant surface potential of the PFA (perfluoroalkoxy [23]) layer that can be derived by the technique introduced in [24]. C_{max} is the maximum capacitance between the top and bottom electrodes when the top electrode is in contact with the dielectric layer and C_{min} is the minimum capacitance when the air gap is at its maximum; the inequality $C_{max} > C_{min}$ hold at all times. Both values of C_{max} and C_{min} can be calculated using the technique described in the supplementary material [25] (also see section S1 of supporting information). The parasitic capacitance of the circuits, C_{par}, is measured using the same technique described in [25]. The value of C_{par} is then subtracted from the values of C_{max} and C_{min} to make them the net capacitance of the TENG. Therefore, the derived equations (1)–(7) below are insensitive to parasitic capacitance.

Since ΔW_{i_HW} is a quadratic function of V_C, there is an optimum V_C^{max} value in which the energy is maximum [22]:

$$V_C^{max} = \frac{1}{2}V_{TE}(C_{max}/C_{min} - 1) \tag{2}$$

Then, the maximum converted energy is found as [22]:

$$\Delta W_{max\_HW} = \frac{1}{4}V_{TE}^2C_{min}(C_{max}/C_{min} - 1)^2 \tag{3}$$

For the case of full-wave rectifier the converted energy during i^{th} cycle of operation is [22] (Section S2 of supporting information):

$$\Delta W_{i\_FW} = 2V_{C\_i}C_{min}(C_{max}/C_{min} + 1)\left(V_{TE}\frac{C_{max}/C_{min} - 1}{C_{max}/C_{min} + 1} - V_{C\_i}\right) \tag{4}$$

and the value of V_C^{max} is found as [22]:

$$V_C^{max} = \frac{1}{2}V_{TE}\left(\frac{C_{max}/C_{min} - 1}{C_{max}/C_{min} + 1}\right) \tag{5}$$

Accordingly, the maximum converted energy is [22]:

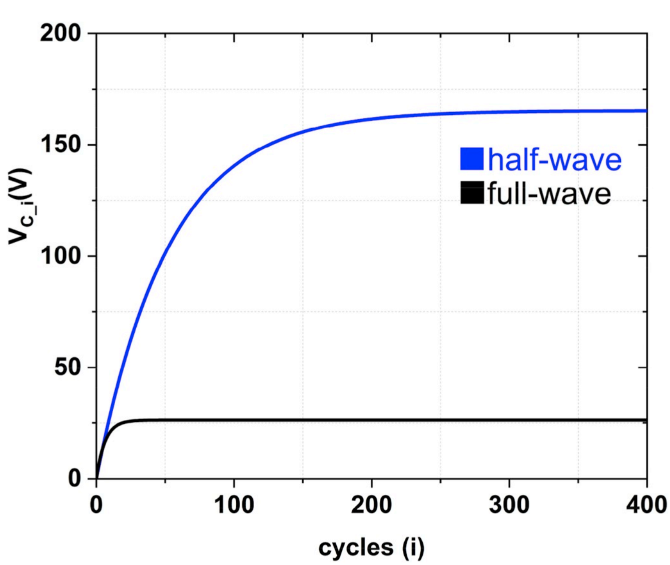

Fig. 2. Measured charging curves of V_{C_i} for half-wave and full-wave rectifiers when working as a conditioning circuit for the TENG.

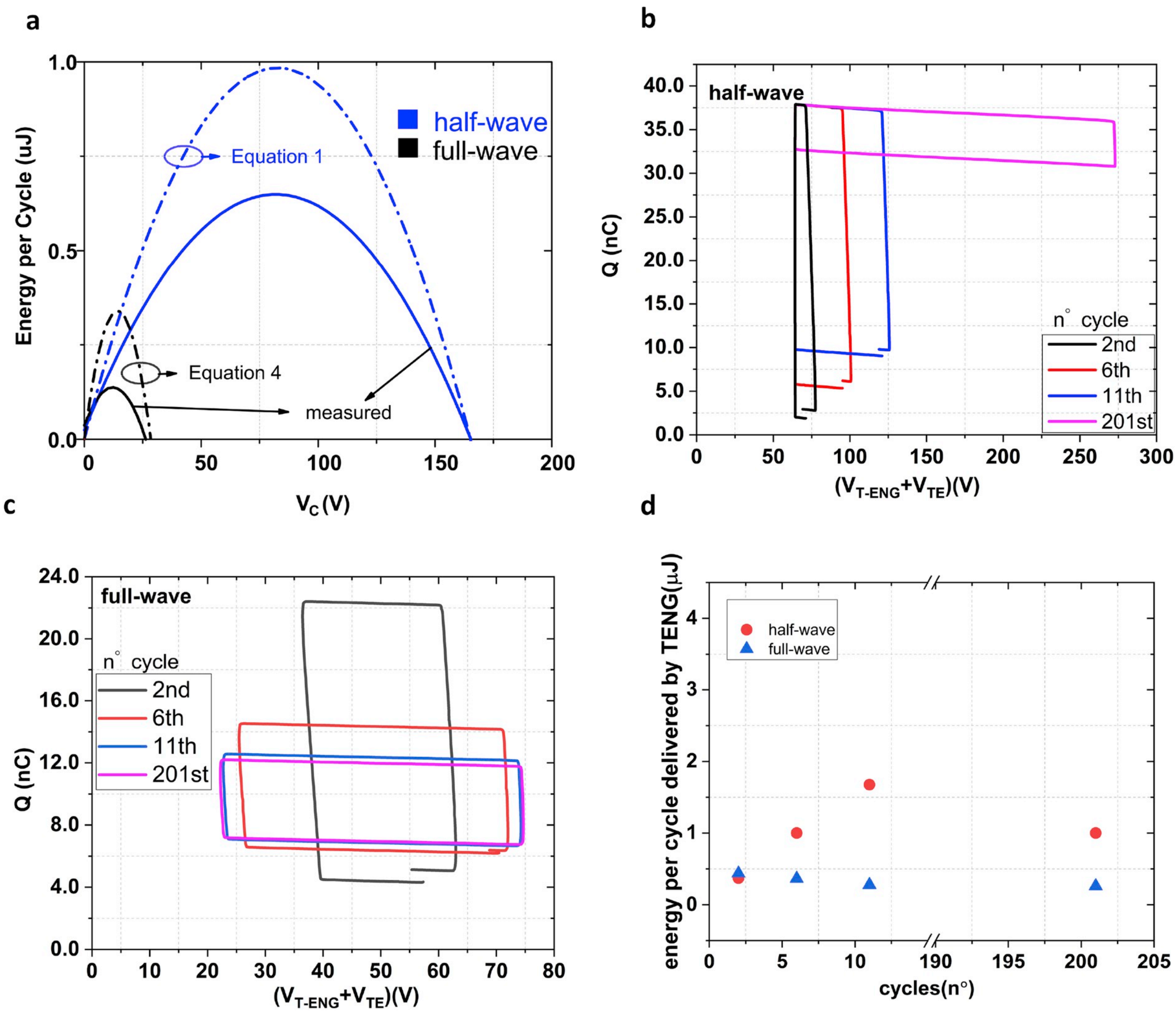

Fig. 3. a. measured and calculated energy delivered to the capacitor C as a function of V_C for the device shown in Fig. 1 with $10 \times 10\,\text{cm}^2$ surface area and periodic excitation of 5 Hz and. b. simulated QV cycles of the TENG for four cycles of operation with half-wave rectifier as the CC. c. simulated QV cycles of the TENG for the same cycles with full-wave rectifier as the CC. d. comparison of calculated energy per cycle delivered by TENG for 2nd, 6th, 11th and 201st cycles of operation corresponding to b and c.

$$\Delta W_{max\_FW} = \frac{1}{2} V_{TE}^2 C_{min} \cdot \frac{(C_{max}/C_{min} - 1)^2}{(C_{max}/C_{min} + 1)} \tag{6}$$

The ratio of the maximum energy of the half-wave over full-wave conditioning circuit gives:

$$r_E = \frac{\Delta W_{max\_HW}}{\Delta W_{max\_FW}} = \frac{1}{2}(C_{max}/C_{min} + 1) \tag{7}$$

Since $C_{max}/C_{min} > 1$, it is observed that half-wave rectifier delivers a higher maximum energy to the load compared to full-wave rectifier.

3. Experimental results and discussion

According to Fig. 1a, a CS TENG is fabricated with a dielectric layer of PFA having 50 μm in thickness, relative permittivity of 2.1 and area of $10 \times 10\,\text{cm}^2$. The TENG is actuated with 5 Hz frequency and is connected in turn to both conditioning circuits of Fig. 1b and c. The output voltage of V_C is measured through a high input-impedance follower.

A maximum contact force of 1.33 N is measured with the force sensor. $C = 4.7$ nF for both circuits using 1N649 diodes with 835 V of measured breakdown voltage. Fig. 2 shows the measured charging curves of capacitance C for both conditioning circuits. Saturation values of V_C for half-wave and full-wave rectifiers are 165 V and 26 V respectively. Values of $C_{max} = 692$ pF, $C_{min} = 144$ pF and $V_{TE} = 43.42$ V are measured.

Fig. 3a shows the calculated energy per mechanical cycle delivered to the capacitance C according to equations (1) and (4), as well as the measured energy as a function of V_C. Both theoretical and measured values verify that the half-wave rectifier delivers a higher maximum energy compared to the full-wave. It also shows that the measured and theoretical curves have a very good overlap for the value of V_C corresponding to the maximum energy. This value is measured as 81.2 V for the half-wave circuit and 12.42 V for the full-wave. Theoretical values from equations (2) and (5) would yield similar values as 82.49 and 14.22 for half-wave and full-wave respectively.

Theoretical curves in Fig. 3a along with equations (3) and (6) verify that the maximum converted energy is 0.98 μJ and 0.33 μJ for half-wave and full-wave rectifiers respectively. This results in a $r_E = 2.96$ from equation (7). On the other hand, measured curves of Fig. 3a have their peaks of energy at 0.64 μJ for the half-wave and 0.13 μJ for the full-wave, which results in a ratio $r_E = 4.92$. Therefore, both experimental and theoretical findings verify the superior performance of the half-wave rectifier over the full-wave when the harvested energy from a TENG is transferred to a capacitive load. It's worth to notice that the deviation between measured energy and theoretical value comes mainly

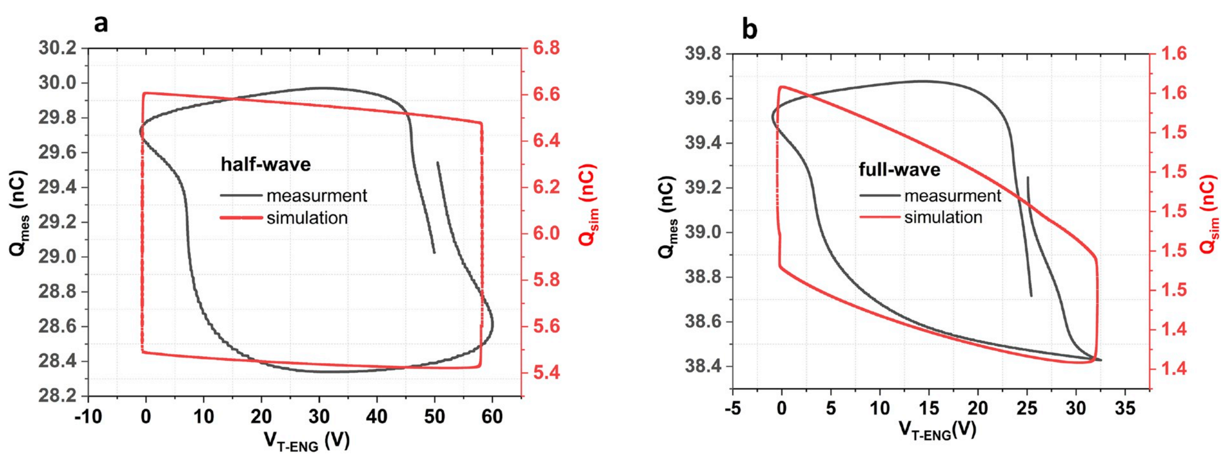

Fig. 4. Measurements and simulations of QV cycles of TENG when connected to: a. half-wave rectifier and b. full-wave rectifier. both QV cycle are measured at 101st cycle of operation of the TENG.

Table 1
Comparison of measured and simulated energy extracted from QV cycle of the TENG with half and full-wave rectifiers.

Energy at 101st cycle (nJ)	half-wave rectifier	full-wave rectifier
measured	61	21
simulated	62	27

from the assumption of ideal circuit elements. Especially, diodes consume energy in both forward and reverse modes for their normal operation, which would result in smaller delivered energy to the capacitance *C*.

Fig. 3b and c shows simulated QV cycles of TENG connected to both CC for the 2nd, 6th, 11th and 201st cycles. The area enclosed by each rectangular indicates the amount of energy delivered by the TENG to the rest of the circuit elements. Use of QV diagram is widespread for the purpose of comparison of output performance of TENG [7,26]. Fig. 3d compares the calculated delivered energy (enclosed area) of corresponding cycles in Fig. 3b and c. This figure also confirms that the TENG delivers a higher maximum energy when connected to the half-wave rectifier compared to full-wave.

4. Comparison of measured and simulated QV cycles

A new CS TENG similar to the device in section 3 is fabricated with smaller dimensions of $5 \times 5\ \mathrm{cm}^2$ and contact force of 0.2 N. Diodes in half-wave and full-wave circuits are replaced with very low leakage diodes of MMBD1501A type and $C = 4.7$ nF. QV cycles of the TENG are measured when connected to each CC. Due to memory limitation on the picoammeter (Keithley 6485) device, current and voltage of the TENG is recorded for only 30 seconds. Fig. 4a and b shows measured and simulated QV cycle of the TENG at 101st cycle of operation corresponding to the time between 20 S and 21 S (corresponding to 5 Hz actuation frequency).

The measured and simulated QV cycles are divided into smaller rectangular in order to calculate the total area enclosed by each curve which corresponds to the converted energy by the TENG. Table 1 compares the results between half-wave and full-wave rectifiers.

Based on the results presented in Table 1, half-wave CC delivers a higher energy to the storage capacitance compared to full-wave CC.

5. Conclusion

Theoretical analysis is performed to compare the performance of half-wave and full-wave rectifiers as conditioning circuits for CS and LS mode TENG, and it is shown that half-wave circuit delivers a higher amount of energy per cycle to a capacitive load compared to full-wave. For both circuits, formulas for the calculation of optimum load voltage and maximum delivered energy are derived, which shows the better performance of the half-wave rectifier. QV cycles of the TENG for both CC are measured and compared with simulation results. Finally, experimental results indicate a very good agreement with the theories and verifies the superior performance of the half-wave rectifier over the full-wave.

Acknowledgment

This work was supported by Iran Ministry of Science, Research and Technology.

Appendix A. Supplementary data

Supplementary data to this article can be found online at https://doi.org/10.1016/j.nanoen.2019.104137.

References

[1] W. Jiang, H. Li, Z. Liu, Z. Li, J. Tian, B. Shi, Y. Zou, H. Ouyang, C. Zhao, L. Zhao, R. Sun, H. Zheng, Y. Fan, Z.L. Wang, Z. Li, Fully bioabsorbable natural-materials-based triboelectric nanogenerators, Adv. Mater. 30 (2018) 1801895, https://doi.org/10.1002/adma.201801895.
[2] G. Zhu, P. Bai, J. Chen, Z. Lin Wang, Power-generating shoe insole based on triboelectric nanogenerators for self-powered consumer electronics, Nano Energy 2 (2013) 688–692, https://doi.org/10.1016/j.nanoen.2013.08.002.
[3] F.-R. Fan, Z.-Q. Tian, Z. Lin Wang, Flexible triboelectric generator, Nano Energy 1 (2012) 328–334, https://doi.org/10.1016/j.nanoen.2012.01.004.
[4] R. Hinchet, A. Ghaffarinejad, Y. Lu, J.Y. Hasani, S.-W. Kim, P. Basset, Understanding and modeling of triboelectric-electret nanogenerator, Nano Energy (2018), https://doi.org/10.1016/j.nanoen.2018.02.030.
[5] A. Karami, D. Galayko, P. Basset, Series-parallel charge pump conditioning circuits for electrostatic kinetic energy harvesting, IEEE Trans. Circuits Syst. Regul. Pap. 64 (2017) 227–240, https://doi.org/10.1109/TCSI.2016.2603064.
[6] A. Ghaffarinejad, J.Y. Hasani, R. Hinchet, Y. Lu, H. Zhang, A. Karami, D. Galayko, S.-W. Kim, P. Basset, A conditioning circuit with exponential enhancement of output energy for triboelectric nanogenerator, Nano Energy (2018), https://doi.org/10.1016/j.nanoen.2018.06.034.
[7] Y. Zi, J. Wang, S. Wang, S. Li, Z. Wen, H. Guo, Z.L. Wang, Effective energy storage from a triboelectric nanogenerator, Nat. Commun. 7 (2016) 10987.
[8] X. Cheng, W. Tang, Y. Song, H. Chen, H. Zhang, Z.L. Wang, Power management and effective energy storage of pulsed output from triboelectric nanogenerator, Nano Energy 61 (2019) 517–532, https://doi.org/10.1016/j.nanoen.2019.04.096.
[9] J. Luo, Z.L. Wang, Recent advances in triboelectric nanogenerator based self-charging power systems, Energy Storage Mater. (2019), https://doi.org/10.1016/j.ensm.2019.03.009. S2405829718314065.
[10] T. He, Q. Shi, H. Wang, F. Wen, T. Chen, J. Ouyang, C. Lee, Beyond energy harvesting - multi-functional triboelectric nanosensors on a textile, Nano Energy 57 (2019) 338–352, https://doi.org/10.1016/j.nanoen.2018.12.032.
[11] A. Ghaffarinejad, Y. Lu, R. Hinchet, D. Galayko, J.Y. Hasani, S.W. Kim, P. Basset, Bennet's doubler working as a power booster for triboelectric nano-generators, Electron. Lett. (2017), https://doi.org/10.1049/el.2017.3434.

[12] L. Xu, T. Jiang, P. Lin, J.J. Shao, C. He, W. Zhong, X.Y. Chen, Z.L. Wang, Coupled triboelectric nanogenerator networks for efficient water wave energy harvesting, ACS Nano 12 (2018) 1849–1858, https://doi.org/10.1021/acsnano.7b08674.
[13] Q. Zhang, Q. Liang, Q. Liao, M. Ma, F. Gao, X. Zhao, Y. Song, L. Song, X. Xun, Y. Zhang, An amphiphobic hydraulic triboelectric nanogenerator for a self-cleaning and self-charging power system, Adv. Funct. Mater. 28 (2018) 1803117, https://doi.org/10.1002/adfm.201803117.
[14] Q. Zhang, Q. Liang, Z. Zhang, Z. Kang, Q. Liao, Y. Ding, M. Ma, F. Gao, X. Zhao, Y. Zhang, Electromagnetic shielding hybrid nanogenerator for health monitoring and protection, Adv. Funct. Mater. 28 (2018) 1703801, https://doi.org/10.1002/adfm.201703801.
[15] A. Proto, M. Penhaker, S. Conforto, M. Schmid, Nanogenerators for human body energy harvesting, Trends Biotechnol. 35 (2017) 610–624, https://doi.org/10.1016/j.tibtech.2017.04.005.
[16] S.K. Ravi, T. Wu, V.S. Udayagiri, X.M. Vu, Y. Wang, M.R. Jones, S.C. Tan, Photosynthetic bioelectronic sensors for touch perception, UV-detection, and nanopower generation: toward self-powered E-skins, Adv. Mater. 30 (2018) 1802290, https://doi.org/10.1002/adma.201802290.
[17] L. Wang, K. Wang, Z. Lou, K. Jiang, G. Shen, Plant-Based modular building blocks for "green" electronic skins, Adv. Funct. Mater. 28 (2018) 1804510, https://doi.org/10.1002/adfm.201804510.
[18] W. Tang, T. Zhou, C. Zhang, F. Ru Fan, C. Bao Han, Z. Lin Wang, A power-transformed-and-managed triboelectric nanogenerator and its applications in a self-powered wireless sensing node, Nanotechnology 25 (2014) 225402, https://doi.org/10.1088/0957-4484/25/22/225402.
[19] G. Zhu, J. Chen, T. Zhang, Q. Jing, Z.L. Wang, Radial-arrayed rotary electrification for high performance triboelectric generator, Nat. Commun. 5 (2014), https://doi.org/10.1038/ncomms4426.
[20] S. Niu, X. Wang, F. Yi, Y.S. Zhou, Z.L. Wang, A universal self-charging system driven by random biomechanical energy for sustainable operation of mobile electronics, Nat. Commun. 6 (2015), https://doi.org/10.1038/ncomms9975.
[21] F. Xi, Y. Pang, W. Li, T. Jiang, L. Zhang, T. Guo, G. Liu, C. Zhang, Z.L. Wang, Universal power management strategy for triboelectric nanogenerator, Nano Energy 37 (2017) 168–176, https://doi.org/10.1016/j.nanoen.2017.05.027.
[22] P. Basset, E. Blokhina, D. Galayko, Electrostatic Kinetic Energy Harvesting, Wiley, Hoboken, NJ, 2016.
[23] Goodfellow Inc, Wholesale and Distribution Company. http://www.goodfellow.com (n.d.).
[24] A. Ghaffarinejad, J. Yavand Hasani, Modeling of triboelectric charge accumulation dynamics at the metal–insulator interface for variable capacitive structures: application to triboelectric nanogenerators, Appl. Phys. A 125 (2019) 259, https://doi.org/10.1007/s00339-019-2495-y.
[25] Y. Lu, E. O'Riordan, F. Cottone, S. Boisseau, D. Galayko, E. Blokhina, F. Marty, P. Basset, A batch-fabricated electret-biased wideband MEMS vibration energy harvester with frequency-up conversion behavior powering a UHF wireless sensor node, J. Micromech. Microeng. 26 (2016) 124004, https://doi.org/10.1088/0960-1317/26/12/124004.
[26] H. Zhang, Y. Lu, A. Ghaffarinejad, P. Basset, Progressive contact-separate triboelectric nanogenerator based on conductive polyurethane foam regulated with a Bennet doubler conditioning circuit, Nano Energy 51 (2018) 10–18, https://doi.org/10.1016/j.nanoen.2018.06.038.

Ali Ghaffarinejad is pursuing his Ph.D. degree under supervision of Professor Javad Yavand Hasani at School of Electrical Engineering, Iran University of Science and Technology (IUST), Tehran, Iran. He is currently a visiting student at ESYCOM lab, Université Paris-Est/ESIEE, Paris, France. He received his B.Sc. degree in Electronic engineering from the University of Kerman, Iran, in 2006, the M.Sc. degree in Bioelectronics from IUST in 2011. His research interests include modeling of triboelectric charge generation and stability in kinetic energy harvesters and RF-MEMS devices. Currently he is focusing on power management circuits for triboelectric-electret energy harvesters.

Dr. Javad Yavand Hasani is a professor in the School of Electrical Engineering at Iran University of Science and Technology (IUST), Tehran, Iran. In 2009 he received the PhD degree in electrical engineering from the University of Tehran and the PhD degree in high frequency and optics from the University of Joseph Fourier (UJF), Grenoble, France. From 2012 to 2014 he was the dean of the Electronic Research Center (ERC) in IUST. His current research interests include high frequency circuits and systems, as well as micro-fabrication theory and technology for RF and microwave devices, MEMS and NEMS.

Dimitri Galayko was graduated from Odessa State Polytechnic University (Ukraine) in 1998, he received his master degree from Institute of Applied Sciences of Lyon (INSA-LYON, France) in 1999. He made his PhD thesis in the Institute of Microelectronics and Nanotechnologies (IEMN, Lille, France) and received the PhD degree from the University Lille-I in 2002. Since 2005 he is an associate professor in University Paris VI (UPMC, Sorbonne Universités) in the Laboratory of Computer Science (LIP6). His research interests cover design and modeling of heterogeneous systems involving a combination of classical CMOS integrated circuit with physical sensors such as MEMS devices and energy harvesters, study of different aspects of oscillating structures in microelectronics (both solid-state CMOS oscillators and MEMS oscillators), and investigation and modeling of nonlinear phenomena emerging in such systems. He is an active member of the Technical Committee Nonlinear Circuits and Systems of IEEE CAS society.

Dr. Philippe Basset is professor at Université Paris-Est / ESIEE Paris. He received his engineering diploma in electronics from ISEN Lille, France, in 1997, his M.Sc and Ph.D from IEMN University of Lille in 1999 and 2003 respectively, in the areas of microelectronic and micro-electro-mechanical-systems (MEMS). In 2004 he was a post-doc at Carnegie Mellon University, Pittsburgh, USA. In 2005 he joined ESIEE Paris at the Université Paris-Est, France. His current research interests include micro-power sources for autonomous sensors and micro/nano-structuration of silicon. He currently serves in the International Steering Committee of the PowerMEMS conference and he is deputy director of the ESYCOM laboratory.